Highlights

An ensemble multi-ANN approach for virtual oxygen sensing and air leakage prediction in biomass gasification plants

Antonio Escámez, Roque Aguado, Daniel Sánchez-Lozano, Francisco Jurado, David Vera

- An ML model has been developed to detect air leakages in biomass gasification plants
- A pilot-scale gasification plant has been used to collect the whole dataset
- The model has been trained on a dataset comprising a total of 27,715 records
- The RMSE of the model is 0.3, below the precision of the sensor used to record data
- The model can be used as a virtual sensor to supervise or replace the real sensor

An ensemble multi-ANN approach for virtual oxygen sensing and air leakage prediction in biomass gasification plants

Antonio Escámez, Roque Aguado*, Daniel Sánchez-Lozano, Francisco Jurado, David Vera

Departamento de Ingeniería Eléctrica, Escuela Politécnica Superior de Linares, Universidad de Jaén, Avda. de la Universidad s/n, 23700 Linares, Spain

Abstract

A recurring challenge in the operation of biomass gasification plants is the occurrence of air leakages, which cause the resulting lean producer gas not to meet the required standards for power generation. In order to address this issue, an ensemble model composed of multiple artificial neural networks (ANNs) was developed to predict the oxygen concentration in the gas mixture and detect anomalous operating conditions (air leakages). Throughout an extensive experimental campaign, the volumetric composition of the gas mixture from a semi-industrial scale downdraft gasifier fueled with biomass pellets was systematically measured and recorded at a constant time step of 10 seconds using an inline portable syngas analyzer equipped with NDIR, TCD and ECD sensors. The ensemble multi-ANN model was trained with a total of 24 representative datasets, including instances of both normal and anomalous operating conditions, using k-fold cross validation with 10 submodels. The results revealed an R^2 of 0.99 and an RMSE below 0.3, indicating that the model's error margin is lower than that of the ECD sensor. The developed model can serve as a supervisor of the ECD sensor by performing a double verification or even potentially replacing the ECD sensor, with the model assuming the task of predicting the oxygen concentration using the data recorded by the NDIR sensor.

Keywords: Downdraft gasifier, Producer gas, Air leakages, Virtual sensor, Artificial neural network, Machine learning

1. Introduction

The escalating global demands for energy, along with the environmental concerns and the pressing need for sustainable waste management methodologies have recently renewed interest in the gasification technology [1, 2]. Through this thermochemical process, solid carbonaceous

*Corresponding author

Email addresses: aescamez@ujaen.es (Antonio Escámez), ramolina@ujaen.es (Roque Aguado), dslozano@ujaen.es (Daniel Sánchez-Lozano), fjurado@ujaen.es (Francisco Jurado), dvera@ujaen.es (David Vera)

feedstocks such as biomass are converted into a combustible gas with diverse end applications, ranging from the combined generation of electricity and heat to the production of synthetic chemicals, including automotive fuels [3–5]. Various gasifying agents, such as air, pure oxygen, steam, carbon dioxide, or combinations thereof, can be used to facilitate the conversion of solid feedstock into combustible gas. However, ambient air is the most commonly used gasifying agent due to its wide availability and low cost. The resulting gaseous product from gasification using air as gasifying agent is a lean fuel gas known as producer gas, which consists of hydrogen (H_2), carbon monoxide (CO), carbon dioxide (CO_2), nitrogen (N_2), methane (CH_4), and lightweight hydrocarbons (C_nH_m). This gas can be used for electricity generation through internal combustion engines, turbines, or fuel cells [2, 6]. Furthermore, producer gas holds substantial potential for combined heat and power (CHP) generation, positioning gasification as a highly attractive option for distributed cogeneration systems [7, 8]. By enabling both electricity and heat production in a single system, biomass gasification CHP systems can deliver efficient, localized renewable energy solutions, particularly in areas where low-cost biomass is readily available as fuel.

Gasifiers are categorized into three main types, namely fixed bed, fluidized bed and entrained flow, each with its own configuration and operational mechanism. Fixed-bed gasifiers are further classified into downdraft, updraft, and crossdraft types. Downdraft gasifiers are the most widespread, accounting for roughly three fourths of all gasifiers marketed commercially [3], and are known for their simplicity, low costs, and adaptability to a wide range of carbonaceous feedstocks. It is well established that the gasification process takes place in four different spatial zones within a downdraft gasifier: drying (dehydration), pyrolysis (devolatilization), combustion (oxidation) and gasification (reduction) [9]. In the drying zone, the carbonaceous feedstock dehydrates due to the heat from the lower zone. Subsequently, in the pyrolysis zone, the dried material heats up in the absence of oxygen, releasing gases and tars that descend into the combustion zone. Just below the pyrolysis zone, the low molecular weight gases, tars, and char products from the pyrolysis reactions receive a certain amount of oxidizer from the downstream combustion zone and

are burned in a phenomenon known as flaming pyrolysis [9]. The combustion zone is responsible for generating the heat required for the other stages of the gasification process. Downstream the combustion zone lies the gasification zone, where a combustible gas is formed through a series of endothermic reactions.

Gasification is a highly complex process that involves multiple variables dependent on each other. Due to the inherent complexity of biomass gasification processes, machine learning (ML), a subset of artificial intelligence (AI), has proven to be an effective tool to analyze large datasets, recognize patterns, and model intricate relationships between variables [10–14]. ML techniques have been widely applied to model various types of biomass gasifiers, with most studies in the literature focusing on fixed-bed gasifiers, particularly downdraft configurations [10, 15–19], although updraft gasifiers [20] and fluidized bed gasifiers [21–24] have also been the subject of some ML modeling efforts. Among the available ML techniques, artificial neural networks (ANNs) stand out for their ability to address the nonlinear and highly variable nature of gasification [16, 25, 26]. As a result, ANNs have become the prevailing ML technique used in modeling gasification processes [15–17, 21–29]. Indeed, ANN models have demonstrated their ability to predict gasification outputs with a reasonably high level of accuracy [25]. Nevertheless, their black box nature and lack of interpretability are significant drawbacks [14, 20, 26, 27].

Among ANN models, previous research has indicated that the overall performance and generalization capacity of ANNs can be significantly enhanced by combining multiple networks into an ensemble [29]. Ensembles enhance performance by combining diverse models, overcoming the weaknesses of individual models while amplifying their strengths. Initially, several individual neural networks are constructed and trained on different subsets of data. These networks are separately trained by feeding data, adjusting weights to minimize prediction errors using optimization techniques like gradient descent [30]. Once trained, these networks are combined into an ensemble using methods such as voting or averaging [29, 31]. Voting involves considering predictions from each network and choosing the most common or weighted prediction, while av-

eraging calculates the mean prediction, which aligns better with models that produce continuous outputs [31]. Averaging methods in ensemble modeling primarily fall into two categories: simple averaging and weighted averaging [29]. Simple averaging ensemble (SAE), also referred to as unweighted or naïve averaging, is the most commonly used method, particularly in neural network applications. In contrast, the weighted averaging ensemble (WAE) builds upon SAE by assigning distinct weights to each base model's output, reflecting their relative importance in contributing to the final prediction. Although widely applied in other domains, SAE and WAE have not yet been explored in predictive modeling for gasification processes [29]. The ensemble approach leverages the diverse strengths of individual networks, resulting in improved predictive accuracy, enhanced robustness against overfitting, and greater generalization capability compared to single ANN models [29, 32, 33]. However, it is noteworthy that ensembles involve certain trade-offs, with one key challenge being interpretability [29]. As ensembles aggregate predictions from multiple models, understanding the underlying decision-making process becomes more complex [29].

Despite being recognized for their ability to enhance predictions and accuracy across various domains, the use of ensemble multi-ANN models in the context of gasification is still in its early stages of exploration and application. Indeed, their specific adoption in modeling gasification processes is still limited and only a few related studies are available in the scientific literature. For example, Kardani et al. [34] focused on using an optimized ensemble soft computing model to simulate municipal solid waste gasification. Their findings revealed that the proposed ensemble modeling approach is a promising alternative to address the complexity of nonlinear thermochemical processes. Furthermore, variable importance analysis identified gasification temperature as the most influential operating parameter. Kim et al. [35] developed an automated machine learning algorithm coupled with cooperative game theory to predict the biomass composition and operating parameters in fluidized-bed biomass gasifiers, with ensemble methods showing the highest accuracy.

Since power generation via gasification requires a highly controlled gas composition, detecting

anomalies in the plant that could alter this composition is crucial. One common issue during plant operation is the occurrence of air leakages into filters and pipelines downstream of the gasifier due to corrosion and wear, potentially leading to imperfect seals at the joints. Sharma [36] outlined strategies for addressing such challenges, including the refabrication of certain failed components, such as the gasifier grate, sand bed filters and pipelines, as well as maintenance and replacement procedures for other components, such as the charcoal filter and the water re-circulation line in the cooling system, to prevent air leakages.

In the event of air leakages, the LHV of the producer gas decreases due to dilution with ambient air, potentially leading to a shutdown of the power generation unit. Although these minor air leaks into the gasification system typically do not easily trigger an explosion, massive air leakages may lead to significant concerns of fire and explosion [37]. Therefore, developing accurate models for timely prediction of air leakages is essential for preventing operational disruptions, safeguarding safety, and maintaining overall system reliability. To this end, this research work presents an ensemble multi-ANN model derived from empirical data collected at a semi-industrial gasification plant fueled with exhausted olive pomace pellets. The ensemble multi-ANN model is designed to predict the oxygen concentration within the producer gas and detect air leakages. The results aim to contribute to the development of the biomass gasification technology by reducing the operation and maintenance (O&M) costs of the plant and maximizing its utilization factor.

The rest of this paper is organized as follows. Section 2 delves into the methodological approach, which includes the characterization of biomass feedstock, detailing the gasification plant and instrumentation, outlining the plant operation procedure, dataset collection, and analysis, and eventually delineating the procedure for developing an ensemble multi-artificial neural network (multi-ANN) model to predict the oxygen concentration in the producer gas and detect potential air leakages. Section 3 presents the results of this work, analyzing the prediction performance of the developed model using diverse metrics, as well as the additive explanations of the impact of each feature on the final prediction. Finally, Section 4 provides some concluding remarks,

discusses challenges and limitations, and offers suggestions for future work.

2. Methodology

The experimental methodology is divided into several parts. Initially, the semi-industrial scale gasification plant is described, including the biomass feedstock and the instrumentation for measuring the producer gas composition. Thereafter, the experimental procedure for plant operation and data collection is reported. Finally, the methodology for development of the ensemble multi-ANN model is reported, including the procedure for data preprocessing, model structure and performance metrics.

2.1. Biomass feedstock

The performance of the gasification process is influenced by the physicochemical properties of the biomass feedstock. Olive pomace pellets were used as feedstock for the gasification plant due to their abundant supply in Mediterranean regions [38]. The physicochemical properties of this biomass feedstock can be consulted in previous works of the authors [19, 38]. Fig. 1 illustrates the size of the olive pomace pellets, displaying their cylindrical shape with lengths ranging from 10 mm to 35 mm and diameters around 10 mm.

Figure 1: A sample of exhausted olive pomace pellets used as feedstock for the gasification plant.

2.2. Plant description and instrumentation

The gasification reactor, identified as number 3 in Fig. 2, is based on a throatless downdraft fixed-bed design with an open top. Externally, the reactor features a stainless steel layer, while internally, it incorporates a refractory ceramic lining, which serves as thermal insulator for temperature control during operation and provides protection against the inherent corrosive effects of the gasification process. The producer gas exits the gasifier through a pipeline at a temperature around 400 °C [38]. The producer gas conditioning process incorporates a wet scrubber, labeled as 4 in Fig. 2. The cooling system composed by the cooling tower and the water tank indicated with numbers 1 and 2, respectively, in Fig. 2. The scrubber removes tar and heavier particles from the gas through a water spray mechanism in a closed-loop system, reducing the gas temperature from approximately 400 °C down to around 40–45 °C [39]. Following the scrubbing process, the conditioning unit is composed of a series of filters labeled as 5, 6, 7, and 8 in Fig. 2 to eliminate moisture and the remaining impurities, ensuring that the resulting producer gas meets the required quality standards for utilization in a downstream power generation unit. Right after the producer gas conditioning unit, a blower, designated as number 9 in Fig. 2, operates to induce a vacuum for air entry into the gasifier. Fig. 2 also shows a flare stack marked as number 10, where the producer

gas is burned to avoid the release of air pollutants such as carbon monoxide and methane into the environment until it has reached a suitable composition for being introduced into a downstream power generation unit.

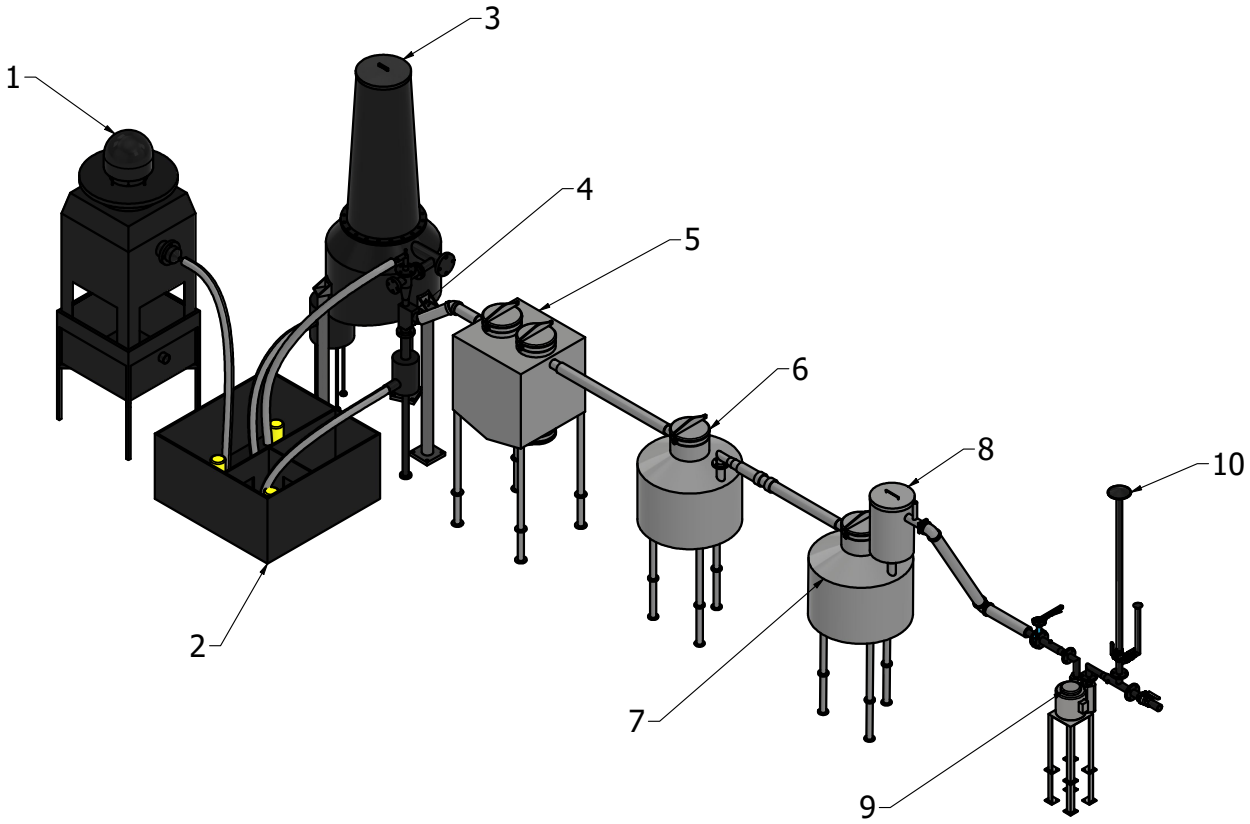

Figure 2: 3D layout diagram of the biomass gasification plant.

For determination of the producer gas composition, a portable syngas analyzer (Gasboard 3100P, Hubei Cubic-Ruiyi Instrument Co., Ltd., Wuhan, China), was used [40]. This instrument incorporates three different sensors to measure the volume concentrations of the main gas species in the producer gas, as outlined in Table 1. Specifically, a non-dispersive infrared (NDIR) sensor is used to determine the concentrations of CO, CO_2, CH_4, and C_nH_m in the producer gas, a thermal conductivity detector (TCD) to measure the concentration of H_2, and an electron capture detector (ECD) to obtain the concentration of O_2.

The operational principle of the syngas analyzer relies on the NDIR spectroscopic sensor for

Table 1: Measurement specifications for each component of the producer gas [40].

Component	Method	Range	Resolution	Precision
CO	NDIR	0–30%	0.01%	≤ 2% Full scale
CO_2	NDIR	0–25%	0.01%	≤ 2% Full scale
CH_4	NDIR	0–10%	0.01%	≤ 2% Full scale
C_nH_m	NDIR	0–5%	0.01%	≤ 2% Full scale
H_2	TCD	0–30%	0.01%	≤ 3% Full scale
O_2	ECD	0–25%	0.01%	≤ 3% Full scale

determining gas concentrations of the major carbon-containing species within the producer gas. Key components of an NDIR spectrometer comprise an infrared light source, an optical tube housing the producer gas, and an infrared detector equipped with a specific wavelength filter [41]. In operation, the NDIR sensor exploits the distinctive absorption wavelengths associated with polyatomic molecular gases within the infrared spectrum.

As the beam of light, featuring the absorption wavelength of the target gas, traverses the gas sample, the gas molecules absorb a fraction of the light, resulting in a reduction of light intensity. The extent of intensity reduction directly correlates with the concentration of the gas in the sample, according to the Beer-Lambert law [42]. This law states that the gas concentration is inversely proportional to the logarithm of the ratio of incident light intensity to transmitted light intensity.

$$I = I_0\, e^{-\varepsilon c l} = I_0\, e^{-A} \tag{1}$$

where:

- I_0: initial light intensity.
- I: light intensity after passing through the gaseous medium.
- A: absorbance.
- ε: absorption coefficient.
- c: gas concentration.
- l: thickness of the gaseous absorption medium.

Accordingly, the absorption intensity (i) of each polyatomic molecular gas can be expressed as follows:

$$i = I_0 - I = I_0\left(1 - e^{-\varepsilon c l}\right) = I_0\left(1 - e^{-A}\right) \tag{2}$$

2.3. Procedure for plant operation and dataset collection

The start-up process begins with a visual inspection of valves positions to direct the producer gas flow toward the flare for combustion. Once the biomass feedstock has been loaded into the gasifier, the blower, pumps, and ancillary motors are activated. Typically, this start-up phase lasts approximately 15 minutes, allowing the producer gas composition to stabilize. Once this steady condition is achieved, the producer gas is rerouted from the flare to the power generation unit.

An example of the temporal evolution in the composition of producer gas generated by the downdraft gasifier during the startup process is illustrated in Fig. 3. It is noticeable that the producer gas generally reaches a stable condition in less than 20 minutes. The decline in oxygen concentration within the producer gas can be explained by the high reactivity of oxygen, which is higher than that of steam and carbon dioxide [9]. Initially, carbon monoxide predominates as the primary fuel component in the producer gas due to the swift kinetics of carbon's partial oxidation into carbon monoxide ($C + {}^1/_2\, O_2 \rightarrow CO$), outpacing other carbon gasification reactions [9]. This reaction rapidly consumes available oxygen, leaving little for other reactions, leading to a peak in carbon monoxide concentration within the producer gas. As shown in Fig. 3, the rise in hydrogen concentration occurs at a slower pace in comparison to carbon monoxide. This phenomenon is attributed to the char–steam reaction's rate, which yields hydrogen ($C + H_2O \rightarrow CO + H_2$), being three to five orders of magnitude slower than that of the char-oxygen reaction [9]. The following decrease in the concentration of carbon dioxide can be partly attributed to the Boudouard reaction ($C + CO_2 \rightarrow CO$), which is six to seven orders of magnitude slower [9]. Among all char gasification reactions, the hydrogasification reaction that yields methane ($C + 2\, H_2 \rightarrow CH_4$) is the slowest. Subsequently, the sharp decrease in carbon monoxide concentration primarily

arises from the increased production of hydrogen and carbon dioxide through the forward water gas shift reaction occurring in the gas phase ($CO + H_2O \rightarrow CO_2 + H_2$) [9]. Consequently, hydrogen concentration rises at the expense of carbon monoxide. The increasing hydrogen concentration also leads to an increase in the methane concentration, mostly attributed to the methanation reactions that convert carbon monoxide into methane ($2\ CO + 2\ H_2O \rightarrow CH_4 + CO_2$, and $CO + 3\ H_2O \rightarrow CH_4 + 2\ H_2O$).

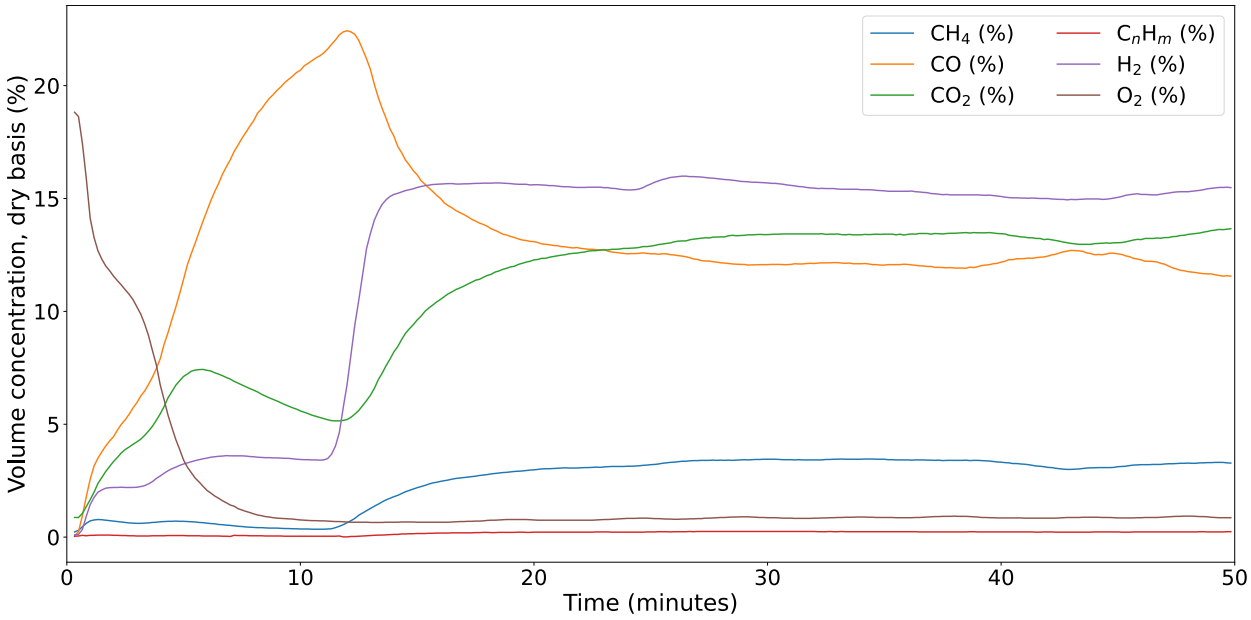

Figure 3: Example of start-up process for the downdraft gasifier, featuring the volume concentrations of measured components within the producer gas during the initial 50 minutes of operation.

The volumetric composition of the producer gas is periodically measured at 10-second intervals by the syngas analyzer and only requires a minimal flow rate of 0.06 m^3/h [38]. Throughout the 24 days of plant operation during the experimental campaign, a dataset comprising a total of 27,715 records was collected, amounting to nearly 77 hours of operation.

2.4. Dataset characterization

Table 2 reports the descriptive statistical analysis of the dataset used to train the ensemble multi-ANN model for predicting oxygen concentration (O_2) based on CO, CO_2, CH_4, and C_nH_m

concentrations. The dataset encompasses a wide range of operating conditions in a gasifier, including steady operation, startup phases, and periods of air infiltration.

The oxygen concentration varies widely, ranging from below 1 vol.% (during gasifier operation under typical conditions) to a maximum of 20.68 vol.% (observed during startups). Since the oxygen concentration in air is approximately 21 vol.%, the oxygen concentration in the producer gas cannot exceed this value. When air infiltrates into the system, it mixes with the producer gas, leading to a dilution effect that reduces the oxygen concentration. However, it is noteworthy that the majority of oxygen concentration values (approximately three-quarters of the data, Q3 according to Table 2) fall below 1 vol.%. These relatively low oxygen concentration values are indicative of normal plant operation, with no significant air leakages. The distribution is heavily right-skewed, with a skewness of 2.89 and kurtosis of 7.32, indicating the presence of occasional extreme values. This is consistent with the maximum observed value of 20.68 vol.% during the startup phase, which is much higher than the median value of 0.87 vol.%. The interquartile range (IQR) of 0.35 vol.% further shows that most data points are clustered near lower concentrations, which correspond to typical operating conditions. However, higher oxygen concentrations may suggest the occurrence of operational issues, such as air leaks. The mean oxygen concentration in the producer gas is 2.04 vol.%, representing the whole dataset, which includes steady operation, startup phases, and several periods of air infiltration during which oxygen concentrations reached around 10 vol.%. This mean value is comparable to the mean oxygen concentration of 2.16 vol.% reported by Ducom et al. [43] for gasification of olive mill solid waste in a pilot-scale downdraft gasifier with three-stage air supply.

Regarding other gas species, CO and CO_2 exhibit similar mean concentrations (~12 vol.%). These concentrations reflect the typical balance between these two gases in the gasification process. However, unlike CO, the distribution of CO_2 is negatively skewed, with a skewness value of -1.42, indicating that lower concentrations occur more frequently than higher ones. Similarly, CH_4 also exhibits a negatively skewed distribution, though to a lesser extent, with a mean value

of 2.64 vol.% and a skewness of −0.65, suggesting that its concentration is generally lower and tends to cluster toward the lower end of the distribution. By contrast, C_nH_m, which include a wide range of lightweight organic compounds (mostly C_2–C_4 hydrocarbons), contribute minimally to the producer gas, with a mean concentration of only 0.17 vol%.

Table 2: Statistical analysis of the whole dataset.

Variable	Volume concentration of each gas species (%)				
	CO	CO_2	CH_4	C_nH_m	O_2
Mean	12.19	12.15	2.64	0.17	2.04
SD [a]	4.14	3.34	1.00	0.07	3.69
CV [b]	0.34	0.28	0.38	0.40	1.82
Min. [c]	0.00	0.00	0.00	0.00	0.15
Q1 [d]	10.36	11.41	2.15	0.13	0.69
Q2 [e]	11.70	13.37	2.79	0.16	0.87
Q3 [f]	14.23	14.36	3.39	0.21	1.04
Max. [g]	28.28	16.89	4.47	0.36	20.68
IQR [h]	3.87	2.95	1.24	0.08	0.35
Skewness	0.21	−1.42	−0.65	0.25	2.89
Kurtosis	1.92	1.12	−0.19	0.03	7.32
MAD [i]	2.90	2.55	0.80	0.05	2.20

[a] Standard deviation, [b] Coefficient of variation, [c] Minimum, [d] First quartile, [e] Median, [f] Third quartile, [g] Maximum, [h] Interquartile range, [i] Median absolute deviation.

Fig. 4 displays the Pearson linear correlation coefficients between all pairs of recorded data in a matrix of plots. The Pearson correlation coefficient for two variables X and Y is given by:

$$r_{XY} = \frac{\sum (X_i - \bar{X})(Y_i - \bar{Y})}{\sqrt{\sum (X_i - \bar{X})^2 \sum (Y_i - \bar{Y})^2}} \tag{3}$$

where:

- r_{XY} is the correlation coefficient between variables X and Y.
- X_i and Y_i are individual values of variables X and Y, respectively.
- $\bar{X}$ and $\bar{Y}$ are the mean values of variables X and Y, respectively.

The resulting correlation coefficient r_{XY} ranges between −1 and 1, where:

- $r_{XY} = 1$ indicates a perfect positive correlation.
- $r_{XY} = -1$ indicates a perfect negative correlation.
- $r_{XY} = 0$ indicates the absence of linear correlation.

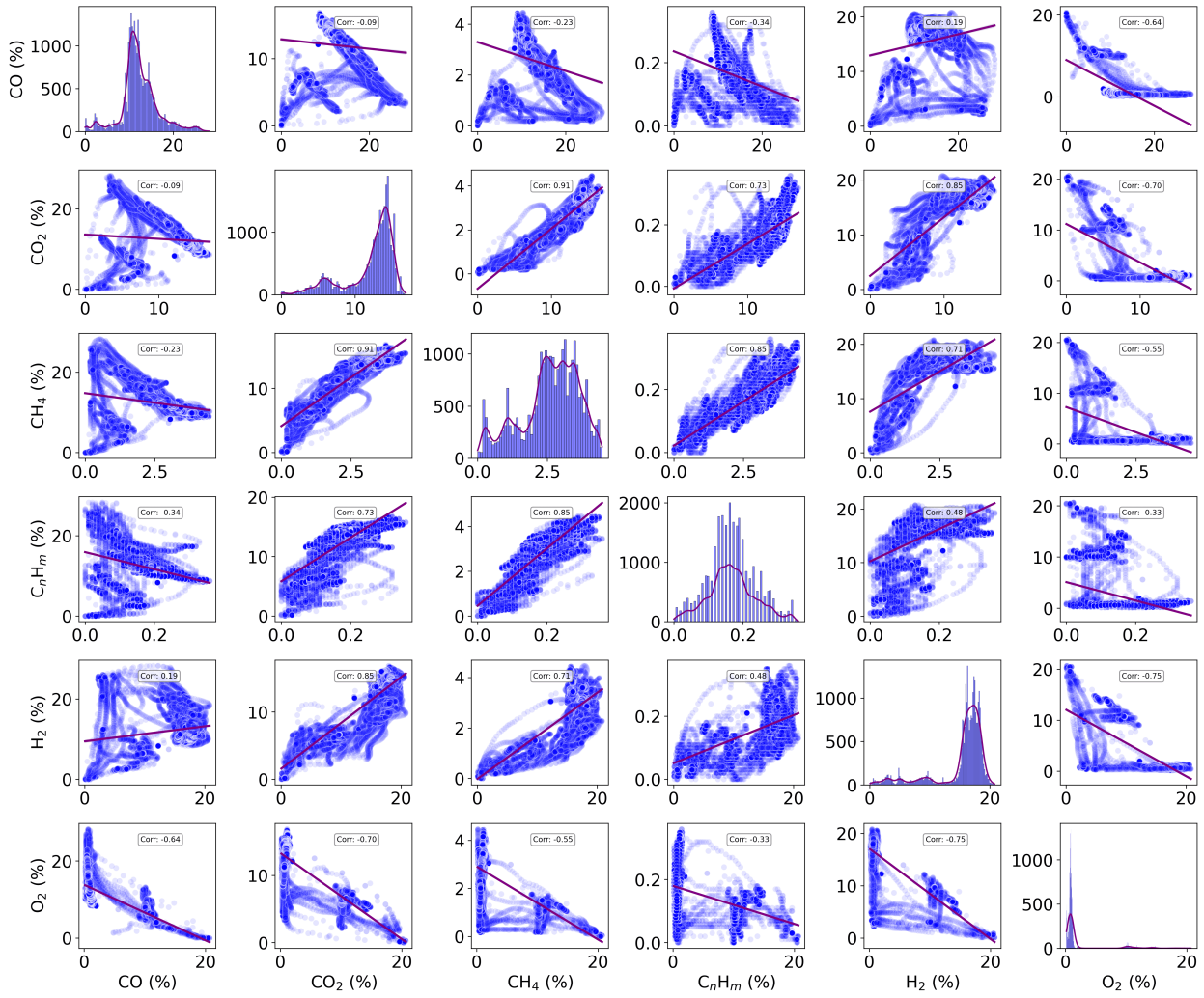

Figure 4: Pearson correlation matrix between all pairs of recorded data.

The main diagonal of the Pearson correlation matrix (Fig. 4) shows the histograms for the volume concentration of each gas species in the producer gas, while scatter plots of all pairs of recorded data appear in the off-diagonal. It is noteworthy that the oxygen concentration tends to cluster below 1 vol.% under normal operating gasification conditions and around 10 vol.% in the presence of air leakages. A strong negative correlation is observed between the volume concen-

tration of oxygen and the volume concentrations of carbon monoxide, carbon dioxide, methane, hydrocarbons, and hydrogen in the producer gas. This is mostly explained by the dilution of the producer gas with air. Indeed, air leakages downstream of the gasifier lead to a higher oxygen concentration, which in turn lowers the concentrations of the other gas components. Since the composition of the producer gas is measured downstream of the gasifier, all oxygen must have already reacted in the reactor according to the equations governing the oxidation zone of the gasification process, such as the complete oxidation of carbon, carbon monoxide, methane and hydrogen as well as the partial oxidation of carbon [9]. Therefore, the monitored oxygen is largely a result of the air leakages occurring between the gasifier outlet and the gas sampling point. This means that, from a chemical reaction perspective, there is no clear conclusion that can be drawn regarding the correlation between the oxygen concentration and the concentrations of other measured gases. The observed negative correlations are not the result of chemical interactions within the gasification process itself. Instead, they are a consequence of the dilution effect caused by the entry of air, which reduces the volume concentrations of the other gases. Furthermore, it is worth noting that the gasification process is inherently dynamic, with variations occurring during both start-up and shutdown phases. Therefore, these correlations should be interpreted within the context of both steady-state conditions and transient fluctuations recorded throughout the whole dataset.

2.5. Development of the ensemble multi-ANN model

This section introduces the procedure for development of an ensemble multi-ANN as a virtual sensor, designed to complement or even potentially replace the ECD sensor in determining the oxygen concentration in the producer gas, as well as detecting air leakages. The model relies only on the data obtained by the NDIR sensor. The model has a dual purpose: it can act as a standalone sensor or complement the ECD as a monitoring tool. The model could detect a failure in the ECD sensor directly by comparing the actual measurements obtained by the ECD with those estimated by the model. If these measurements maintain a sustained difference over time, an alert could be issued, indicating a possible sensor failure. The model is unaffected by failures in the TCD sensor,

since it is not used in its predictions.

2.5.1. Data preprocessing

During the consolidation of datasets into a unified dataframe, certain columns were excluded due to their perceived irrelevance in predicting the oxygen volume concentration, like timestamp. Additionally, calculated values, such as LHV (MJ/m^3) and N_2 concentration, were omitted in favor of focusing on direct measurements. Despite the recording of H_2 concentration data, it was excluded from the ensemble multi-ANN model due to the requirement for a specialized TCD sensor. The preprocessing stage resulted in a dataset that was then partitioned into training, validation, and testing sets, with the oxygen volume concentration identified as the target variable for prediction.

Fig. 5 shows that during the preprocessing stage, a total of 24 datasets were managed. Among these, 21 were merged and shuffled to form the training, validation, and first test dataset. From this combined dataset, 80% was allocated to the training and validation process, and the remaining 20% was set aside for testing. Before the training phase, *k*-fold cross-validation strategy with 10 folds was implemented to enhance the robustness and generalization capability of the ensemble multi-ANN model, and the testing phase was conducted subsequently. The three remaining datasets were intentionally set aside for a second test, introducing operational conditions that deviated slightly from those encountered during the training of the model to ensure robust generalization. Notably, one of these files included air leakages to test the model's ability to discern both normal and anomalous operational conditions. The remaining datasets comprised operational records where the process had deviated slightly from nominal functioning. These deviations included slight changes in the distribution of biomass particle sizes or instances where the reactor did not reach the required temperature, resulting in minor variations in gas composition. Each submodel was trained and validated using 90% of the 80% training dataset (72% of the full dataset), with testing performed on the remaining 10% of this subset (8% of the full dataset). A second validation was carried out using the remaining 20% of the entire dataset to ensure a robust evaluation of the model.

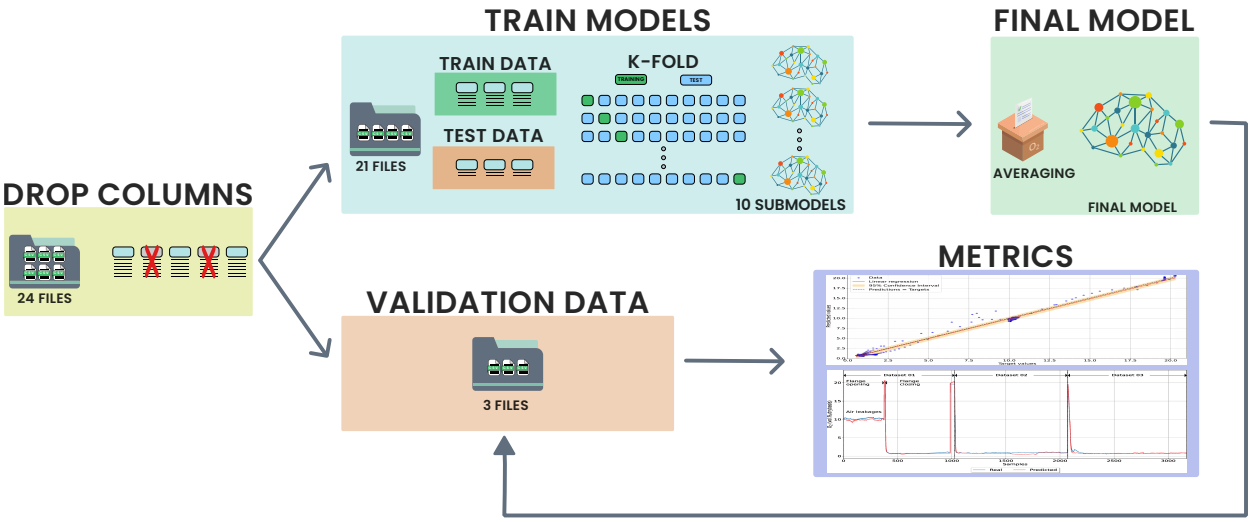

Figure 5: Graphical overview of data preprocessing, training, testing and validation of the ensemble multi-ANN model.

Fig. 6 illustrates the relative distribution of the input parameters to the developed ensemble multi-ANN model. In Fig. 6a, the histogram displays input parameters from datasets used for training the model with *k*-fold cross-validation and the initial test. By contrast, Fig. 6b shows the input parameters used only in a second test, which deviate slightly from the relative distribution used in model training. The input distribution data from the second dataset can be categorized as boundary data, representing the maximum allowable deviations in gasification for process stability. Greater deviations in these parameters would suggest improper operation of the gasification process, with the resulting gas unsuitable for use in the power generation unit. This dual test facilitates the assessment of the model's ability for generalization and avoids overfitting to the initial dataset.

2.5.2. Model structure

Numerous empirical studies have been conducted to quantify the influence of the number of submodels used in building an ensemble [44, 45], with the ensemble size of models or classifiers ranging from ten members to hundreds, and in certain instances, extending up to ten thousands [31]. In this work, ten distinct submodels were created to minimize the computational time and

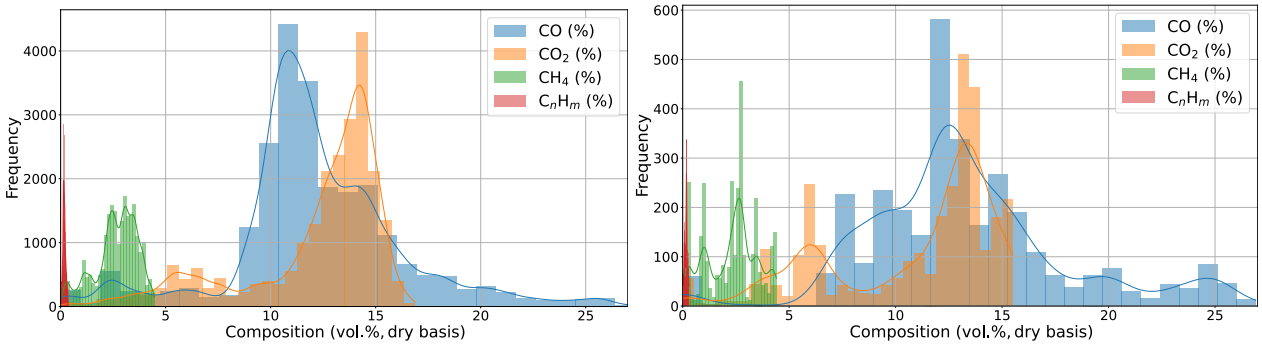

(a) Dataset used in training, cross-validation and test.

(b) Dataset only used in a second test.

Figure 6: Histograms of the datasets used for training, validation and test.

ensure sufficient generalization capability. Each submodel was trained on a different subset of the data. A simple averaging ensemble (SAE) was implemented by averaging the predictions from each individual submodel to determine the final predicted value. This ensemble approach helps mitigating the impact of submodel variability and enhances the overall predictive performance by considering the collective intelligence of multiple submodels. This ensures a more robust and accurate prediction for the target variable (O_2 volume concentration) by leveraging the diverse perspectives of each submodel in the ensemble.

A feed-forward ANN with the multilayer network is a robust tool for non-linear regression analysis [23]. The developed ensemble multi-ANN model consists of 10 neural network submodels, each having a configuration called multilayer perceptron (MLP). As illustrated in Fig. 7, each submodel features an input layer with 4 neurons. It also includes two hidden layers containing 64 and 32 neurons, respectively, both using the rectified linear unit (ReLU) activation function [46]. ReLU was selected due to its simplicity, computational efficiency, and ability to mitigate the vanishing gradient issue, which is commonly encountered with other activation functions such as sigmoid or tanh. ReLU allows faster convergence and more effective training by maintaining a non-linear relationship between the inputs and outputs while avoiding the saturation regions seen in sigmoid or tanh functions [47, 48]. Moreover, the sparse activations used by ReLU contribute to improved model efficiency and generalization [47]. Unlike the hidden layers, the output layer uses

a linear activation function, aligning with the design of other related ANN models in the context of biomass gasification processes [16, 34].

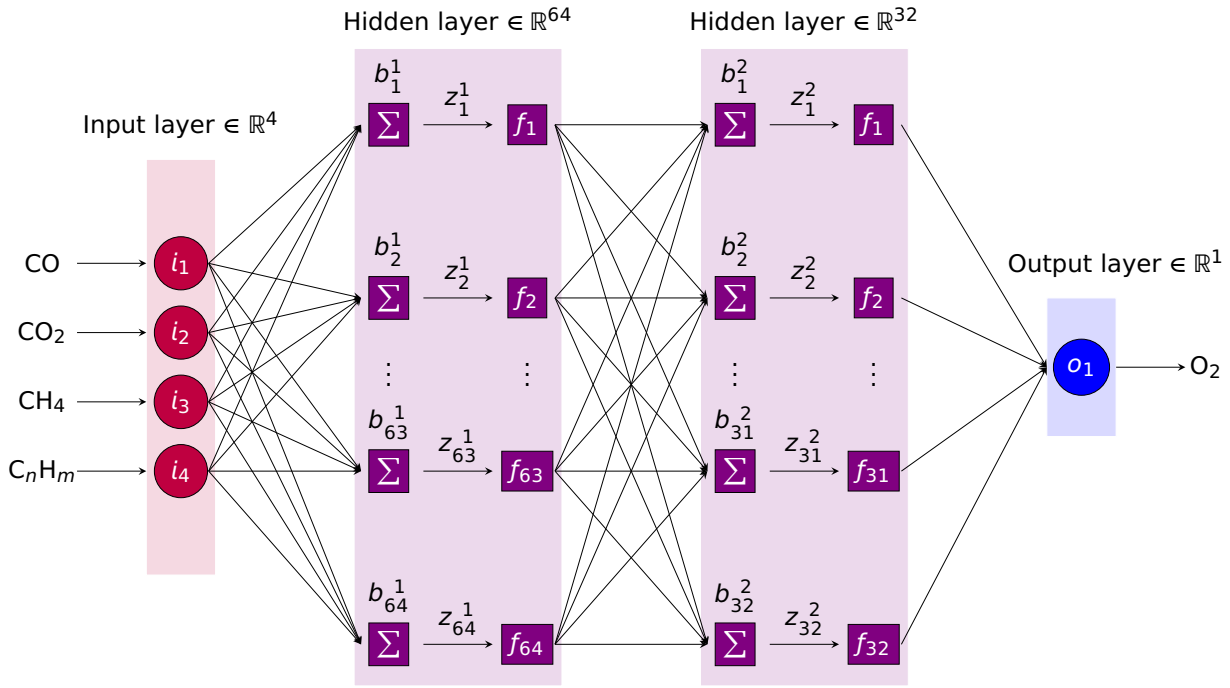

Figure 7: Structure of an MLP submodel to predict the oxygen concentration in the producer gas from a biomass gasification plant. The number of neurons in the hidden layers is reduced for simplicity, intentionally diverging from actual numbers to avoid an overwhelming detail on interconnections.

The fundamental operation of an MLP neural network starts with initialization, setting initial weights and biases. Usually, weights are initialized randomly. This is followed by forward propagation, where the input data passes through the network layer by layer [49]. A neural network of L layers is assumed, excluding the input layer. This structure comprises $L-1$ intermediate or hidden layers and a single output layer. The activation of an intermediate layer l with $l \geq L$ is calculated using the following equation [50]:

$$a^l = f\left(w^l a^{l-1} + b^l\right) \tag{4}$$

In a neural network layer, w^l represents the weight matrix responsible for performing the summation of the outputs a^{l-1} from layer $l-1$ and transmitting them to layer l. Similarly, b^l denotes

the column matrix of biases associated with layer l. The activation function is typically designated as f, which is applied to the intermediate quantity $z^l = w^l a^{l-1} + b^l$. It introduces non-linearity to the network, enabling it to model complex patterns and relationships within the data, which would otherwise be unattainable with linear transformations alone.

If the intermediate quantity obtained by applying the summation is represented by

$$z^l = w^l a^{l-1} + b^l \tag{5}$$

then, the activation of layer l becomes

$$a^l = f(z^l) \tag{6}$$

The summation in neuron i of layer l is given by

$$z_i^l = \sum_j w_{ij}^l a_j^{l-1} + b_i^l \tag{7}$$

where z_i^l denotes the aggregated input to the activation function of neuron i in layer l [51].

Using a loss function to evaluate the difference between the predicted and actual outputs measures the accuracy of the network. Backpropagation then computes the partial derivatives of the loss function, which facilitates adjusting weights and biases to minimize loss. Optimization algorithms such as gradient descent adjust weights and biases to minimize loss functions and improve performance.

$$\frac{\partial C}{\partial w_{jk}^l} \tag{8}$$

$$\frac{\partial C}{\partial b_j^l} \tag{9}$$

where C is the result of the loss function used in the model.

The process of updating the weights of a neural network using gradient descent involves adjusting the weights and biases in the direction opposite to the slope of the cost function (C). The goal is to minimize the cost function and improve the performance of the model.

The bias and weight values are updated according to Adam's algorithm [52], a gradient-based optimizer specifically designed for training neural networks in deep learning. The Adam optimizer was chosen for its efficiency and adaptive learning rates, which enhance convergence by using moving averages of the gradients' first and second moments [53]. It also effectively handles sparse gradients and incorporates bias correction, making it well-suited for large-scale problems [53, 54]. Moreover, Adam requires less hyperparameter tuning compared to SGD and RMSprop, contributing to its widespread adoption [55].

The general rules for updating weights and biases are w^l_{jk} for weights and b^l_j for biases of plane l:

$$w^l_{jk} \leftarrow w^l_{jk} - \eta \frac{\partial C}{\partial w^l_{jk}} \qquad (10) \qquad\qquad b^l_j \leftarrow b^l_j - \eta \frac{\partial C}{\partial b^l_j} \qquad (11)$$

where:

- η is the learning rate, which controls how much the weights are updated at each iteration.
- $\frac{\partial C}{\partial w^l_{jk}}$ is the partial derivative of the cost function with respect to the weight w^l_{jk} and how the cost function changes indicates that this specific gravity changes.
- $\frac{\partial C}{\partial b^l_j}$ is the partial derivative of the cost function with respect to the bias b^l_j and describes how the cost function changes if this particular bias changes. Indicates whether the change will occur.

These updates are performed repeatedly during the training of the neural network, gradually improving the model's performance by reducing the cost function and refining the predictions.

2.5.3. *Performance metrics*

The performance of the ensemble multi-ANN model was evaluated using three scale-dependent performance metrics, namely mean squared error (MSE), root mean squared error (RMSE), and mean absolute error (MAE) [24, 56, 57]. Eqs. (12), (13) and (14) indicate how each error is calculated [26]. A comprehensive review on prediction errors is provided by Shcherbakov et al. [58]. The goodness of fit coefficient, also known as *R*-squared (R^2) score, is also calculated in accordance with Eq. (15).

$$\text{MAE} = \frac{1}{n}\sum_{i=1}^{n}|y_i - \hat{y}_i| \tag{12}$$

$$\text{MSE} = \frac{1}{n}\sum_{i=1}^{n}(y_i - \hat{y}_i)^2 \tag{13}$$

$$\text{RMSE} = \sqrt{\frac{1}{n}\sum_{i=1}^{n}(y_i - \hat{y}_i)^2} \tag{14}$$

$$R^2 = 1 - \frac{\sum_{i=1}^{n}(y_i - \hat{y}_i)^2}{\sum_{i=1}^{n}(y_i - \bar{y})^2} \tag{15}$$

where:

- y_i: Actual values or observations for a specific data point.
- $\hat{y}_i$: Predicted values corresponding to the observed values.
- $\bar{y}$: Mean of the observed values in the dataset.
- n: Total number of observations or data points.

Smaller values of MAE, MSE, and RMSE indicate greater prediction accuracy, whereas a higher R^2 value signifies improved prediction performance [59].

2.6. *Feature importance analysis*

SHapley Additive exPlanations (SHAP) is a powerful method for explaining the output of any machine learning model. It is based on cooperative game theory and assigns each feature a Shapley

value, representing its contribution to the model's prediction [27, 29, 59, 60]. The Shapley value is calculated by considering all possible combinations of features and their impact on the prediction. The Shapley value (ϕ_i) for a specific variable (x_i) is calculated using Eq. (16) [59].

$$\phi_i = \sum_{S \subseteq N \setminus \{i\}} \frac{|S|!(|N| - |S| - 1)!}{|N|!} [f(S \cup \{i\}) - f(S)] \tag{16}$$

where:

- N is the set of all variables.
- S is a set of variables excluding x_i.
- $f(S)$ is the model prediction for the set of variables S.
- $|S|$ is the size of the set S.

The Shapley value for a specific variable is the weighted sum of all prediction differences when adding the variable x_i to different sets of variables S, weighted by the number of ways each set S can be formed. This formula allows to quantify the contribution of each variable to the model's prediction and is particularly useful for interpreting and explaining machine learning model outputs.

SHAP can be used as a global method for describing the average impact of features on an output, as well as a local method for explaining individual predictions [27]. Shapley values are model-agnostic and provide a fair way to distribute the prediction value among the features. The Shapley value of a feature is the average contribution it makes to all possible feature combinations. The influence of input variables on model outputs can be assessed using other feature importance algorithms such as Garson's algorithm [61], which relies on the neural net weight matrix. This algorithm for feature importance analysis has been used in related papers about ANN modeling of biomass gasification processes [14, 16, 17, 24, 62]. However, the choice of SHAP over Garson's algorithm is justified by its model-agnostic nature, which allows it to be applied to a wide range of machine learning models beyond neural networks. By contrast, Garson's algorithm is limited

to use in ANN models with only one hidden layer and may result in incorrect estimates of variable importance [63]. Moreover, Shapley values are based on game theory, providing a fair and consistent measure of feature importance. Another advantage of SHAP over Garson's algorithm is that not only informs about the importance of features, but also their relationship with the output [27]. This versatility and theoretical foundation make SHAP a more comprehensive and reliable tool for understanding the impact of features on model predictions.

3. Results and discussion

This section presents a detailed exploration of the results obtained from the ensemble multi-ANN model, focusing on feature importance analysis, oxygen concentration prediction tests, and performance metrics. The ensemble multi-ANN model's ability to interpret complex relationships within the gasification process is elucidated through the SHapley Additive exPlanations (SHAP) method. The subsequent discussion delves into the model's prowess in predicting oxygen concentrations under various conditions, including air leakages. To quantify its overall performance, key metrics and evaluations are presented subsequently.

3.1. Feature importance analysis

The SHapley Additive exPlanations (SHAP) method is used to interpret the outcomes of the ensemble multi-ANN model. This interpretative approach aids in understanding the relative contributions of each feature (or variable) to the model's predictions for a given data point, which is particularly useful for unraveling the black-box nature of ensemble models. The analysis results are visually represented in Fig. 8, where the abscissa axis illustrates the importance of each feature, and the ordinate axis displays the input features of the ensemble multi-ANN model (specifically, volume concentrations of CO_2, CO, CH_4, and C_nH_m). The features are arranged by overall importance, and the color of the points represents the values of those features, with red indicating higher feature values [64].

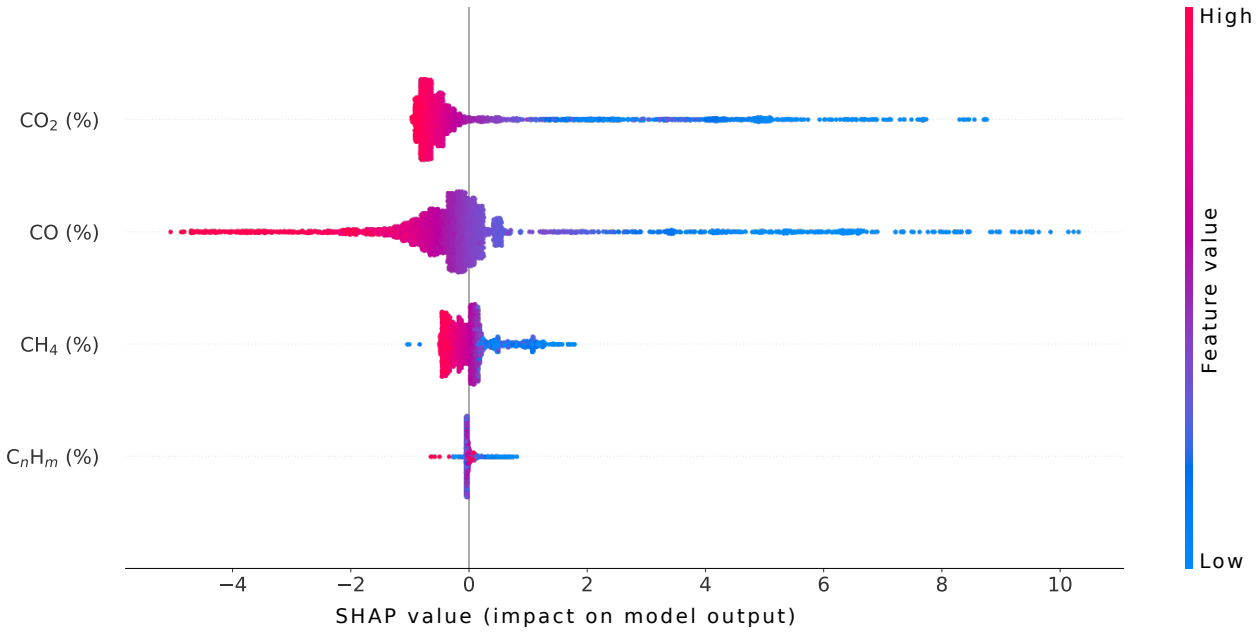

Figure 8: Feature importance analysis for the model predictions using SHapley Additive exPlanations (SHAP) of the trained ensemble multi-ANN model. The color of the points shows the value of those features (red indicates a high feature value).

Fig. 8 shows that a considerable decrease in O_2 content occurs at high CO concentrations, indicating a negative correlation between these two variables. Similarly, elevated CO_2 concentrations are associated with lower O_2 contents. Justification is provided by this alignment with the reactions taking place in the gasifier. It demonstrates the model's capacity to understand the intricate relationships based on the chemical reactions seen in the system and shows that it has successfully inferred the knowledge and interrelationships of the process. By contrast, it is evident that C_nH_m compounds have negligible impact on prediction of the O_2 content.

3.2. Oxygen concentration prediction test

As mentioned above, three distinct datasets were intentionally held separate from the training process. Notably, one of these three datasets contains air leakage data. Fig. 9 visually depicts the model's adeptness in predicting the oxygen concentration under different conditions, including both normal operating scenarios and instances characterized by air leakages.

In the first dataset, an air leakage event is captured due to an improperly sealed flange in the

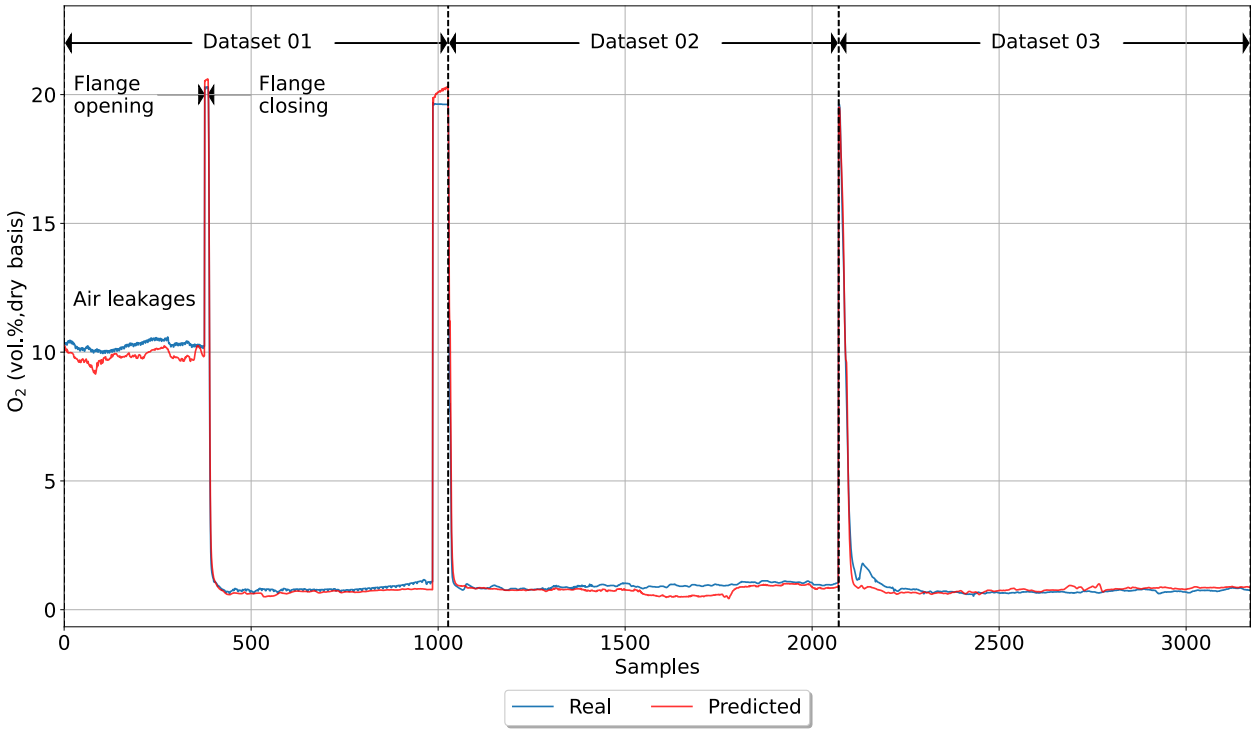

Figure 9: Results from the oxygen concentration prediction test.

cleaning system, resulting in an oxygen concentration in the producer gas around 10% by volume. It is noteworthy that as the flange seal is opened, the oxygen concentration steadily increases until it reaches the composition of the surrounding air. Conversely, upon proper resealing of the flange, the oxygen concentration in the producer gas promptly returns to its normal operating value. This capability of the model to discern and predict fluctuations in oxygen concentration during air leakage events demonstrates its practical utility in real-time monitoring and detection.

The remaining two datasets show the model's performance under normal plant operation conditions. These instances begin with an oxygen concentration slightly above 20 vol.% (representative of air composition) and subsequently decrease to values below 1 vol.%. This behavior aligns with the expected patterns in a well-functioning gasification plant.

It should be noted, that while most of the observations lie in this 0–1 vol.% range for oxygen concentration, sporadic outliers of the order of about 20 vol.% are attributed to gasifier startup events as evidenced in Fig. 10. During start-up, the producer gas composition in the gasifier is

mostly air, which has an oxygen concentration around 20 vol.%. The transitional period can explain the few values between 20 vol.% and 1 vol.%, while the producer gas formation is increasing and the volume fraction of air in the pipelines is decreasing. The large amount of data having an oxygen concentration around 10 vol.% cannot be justified by the aforementioned transitional stage, this grouping of data implies that the composition has been maintained over time, which can only happen if there is a mixture between producer gas and air, which, in turn, involves the presence of air leakage.

The average RMSE value across these three datasets is quantified at 0.3, which surpasses the reported accuracy of the ECD sensor, as previously reported in Table 1.

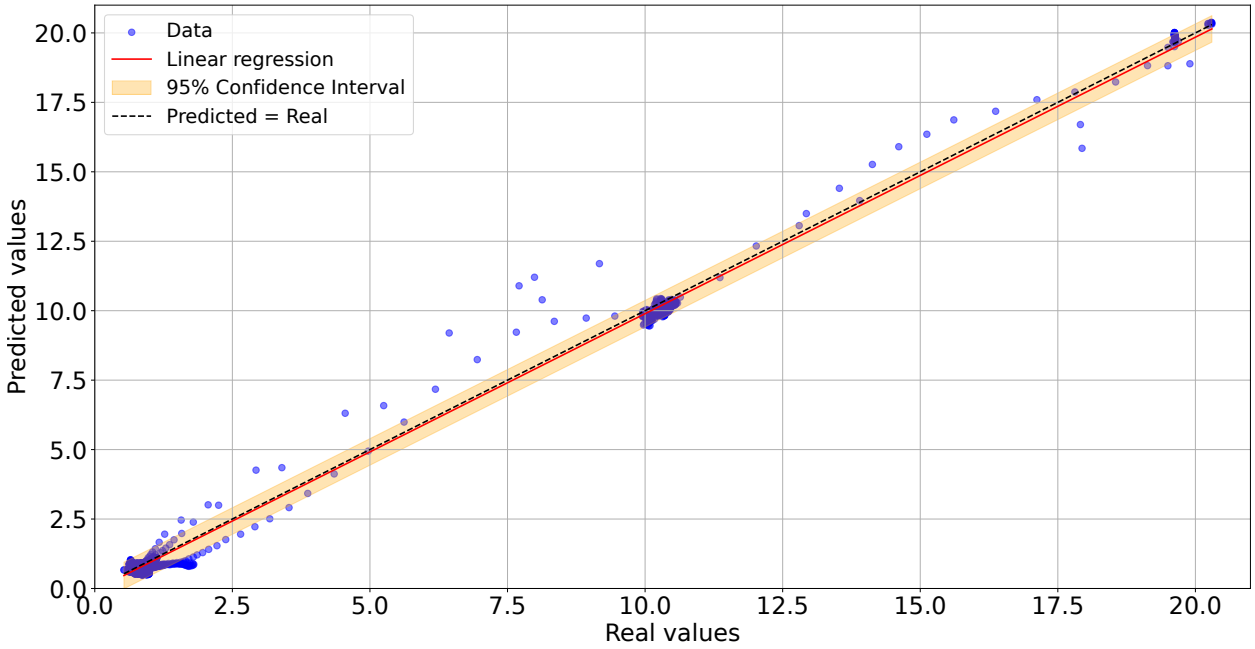

Figure 10: Goodness of fit (R^2) of the real data with the developed ensemble multi-ANN model.

The ensemble multi-ANN model has an R^2 score of 0.99, meaning that it can explain around 99% of the oxygen concentration. The model ability to accurately predict oxygen concentration in gas products along with evidence showing a correlation between oxygen content and system leakages (as shown in Fig. 9) gives it a dual functionality, can be used as a virtual sensor to predict the oxygen concentration and also can be work as a leakage detector due to the proportional

relationship between oxygen and air leakages.

3.3. Performance metrics

The performance evaluation of the ensemble multi-ANN model, illustrated in Fig 11, reveals a noteworthy consistency between its performance on the training and test datasets. The absence of a substantial disparity between the training and test metrics suggests that the model exhibits no signs of overfitting and possesses a commendable ability to generalize effectively to new data that has not been part of the training set. To further validate its generalization capabilities, the model has undergone a second test, producing metrics closely aligned with those obtained in the initial test. This robust performance underscores the model's capacity to make accurate predictions without being excessively adapted to the training data. It is important to clarify that the overarching model uses the 10 submodels shown in Fig. 5 collaboratively, not as independent models. These submodels, work together to produce the final prediction.

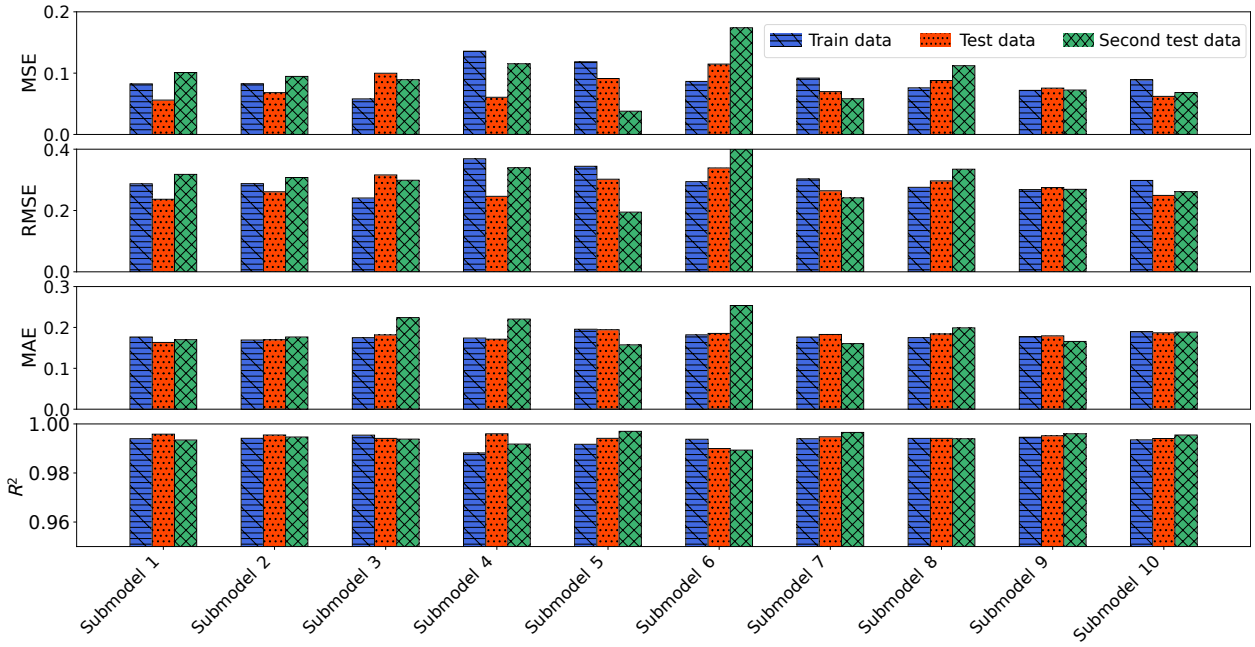

Figure 11: Performance metrics of the ensemble multi-ANN model with train data, test data and second test data.

The RMSE of 0.3 highlights the model's precision in predicting oxygen concentrations. RMSE is particularly useful for comparing the error with the precision of the syngas analyzer because it

brings the error metric back to the original units of the target variable. This makes RMSE more interpretable and easier to understand, as it represents the average magnitude of the error in the same units as the output. In contrast, the ECD sensor, used for measurements, has a precision of 3% within a measurement range of 0–25 vol.%, indicating a maximum margin of error of 0.75 vol.%. Notably, the model's error margin proves to be smaller than that of the sensor, indicating a superior level of accuracy. However, it is imperative to acknowledge that the precision limitations inherent to the ECD sensor inevitably constrain the overall accuracy potential of the model, as the model's predictions cannot surpass the precision threshold set by the sensor.

4. Conclusions, limitations and future developments

The developed ensemble multi-ANN model has proven to be an effective tool in predicting the oxygen concentration in the producer gas and detecting air leakages in a biomass gasification plant. The model achieved high accuracy, with a coefficient of determination (R^2) of 0.99, indicating its ability to explain nearly 99% of the oxygen concentration. The feature importance analysis, using SHAP values, provides valuable insights into the relationships between the oxygen concentration and those of the other main gas species, aligning with chemical reactions within the gasifier. This not only enhances the understanding of the complex processes involved but also validates the model's interpretability and its ability to capture the underlying mechanisms governing oxygen content in the producer gas from biomass gasification. Empirical validation demonstrated the model's capacity to predict the oxygen concentration accurately, maintaining a direct association with oxygen content and air leakages in the system. Performance metrics revealed a root mean squared error (RMSE) of 0.3, which is lower than the precision of the ECD sensor used for measurements. This suggests that the model's performance is surpassing the sensor's precision, making it a valuable tool for predicting and monitoring oxygen leakages in the gasification plant. Trained solely with the data obtained from the NDIR sensor, the model's virtual sensor capabilities allow for the potential elimination of the real ECD sensor, thereby reducing costs and

potential points of failure in the system by relying on a single sensor. This dual functionality of the ensemble multi-ANN model as oxygen predictor and air leakage detector offers opportunities for improved plant reliability, minimized O&M costs. The developed model also contributes to enhanced safety in biomass gasification processes by addressing the risks associated with elevated oxygen concentrations, which might potentially lead to explosions.

Overall, the model's robust performance and ability to generalize well with new data suggest its significant potential to enhance the efficiency and reliability of biomass gasification plants. Implementing the model as a proactive alert system could maximize plant availability and ensure safe and efficient operation of the downstream power generation unit.

4.1. Challenges and limitations

The dataset used for training and validation spans a full year of operation, capturing a broad spectrum of conditions encountered during gasifier operation, including variations in external ambient air temperature, moisture content, and composition of the olive pomace pellets, as well as fluctuations in reactor temperature, among others. The developed model is robust and performs reliably under these specific operating environments. However, the model's performance with other biomass types or with different reactor types, has not yet been assessed and remains a limitation of this study.

Additionally, the model does not directly use input data such as biomass composition (ultimate and proximate analysis), the air-to-fuel stoichiometric ratio (equivalence ratio), or the temperature profile along the reactor's height. Incorporating these inputs would likely enhance the model's ability to generalize. However, the exclusion of these parameters is mainly due to the high cost and effort involved in obtaining them. In most cases, parameters like biomass composition, equivalence ratio, and temperature profile are difficult to measure directly in real-time during operation. Consequently, the model was trained using real, measurable data without relying on indirect measurements. This approach reduces operational complexity and ensures that, during deployment, end users can easily measure the required variables. Continuous monitoring of parameters like the

proximate and ultimate analysis of biomass is not feasible for most end users, which is why the model was designed to work with more readily available and practical data.

All these aspects, along with its scalability to different gasification scenarios, such as varying gasifier sizes or alternative reactor technologies, remain an area of ongoing research that requires further evaluation.

4.2. Future developments

In future research endeavors, it is suggested to find a threshold value that triggers an alert upon surpassing certain limits of oxygen concentration. This early warning system aims to prevent unplanned shutdowns and maximize the availability of the gasifier. These alerts may be confirmed or refuted by the plant operator according to their knowledge, generating a database that can be utilized as feedback for training the model. The following work in this regard is to enable the model to autonomously monitor the power generation unit for instances when it stalls due to air leakages. The suggested improvement involves automatically establishing and adjusting threshold values, thus optimizing the detection of air leakages that lead to unplanned shutdowns of the power generation unit.

CRediT authorship contribution statement

A. Escámez: Conceptualization, Data curation, Formal analysis, Investigation, Methodology, Software, Validation, Visualization, Writing – Original Draft, Writing – Review & Editing. **R. Aguado:** Conceptualization, Formal analysis, Investigation, Methodology, Visualization, Writing – Original Draft, Writing – Review & Editing. **D. Sánchez-Lozano:** Formal analysis, Investigation, Methodology, Visualization, Writing – Review & Editing. **F. Jurado:** Funding acquisition, Resources, Supervision. **D. Vera:** Funding acquisition, Investigation, Methodology, Project administration, Supervision, Validation.

Declaration of competing interest

The authors declare no known personal or financial competing interest.

Funding

Roque Aguado, Antonio Escámez, and Daniel Sánchez-Lozano gratefully acknowledge financial support from *Ministerio de Ciencia, Innovación y Universidades* (Spain) under the FPU Program (Refs. FPU19/00930, FPU22/00741, and FPU22/00879, respectively).

Nomenclature

Abbreviations

AI Artificial intelligence

ANN Artificial neural network

CHP Combined heat and power

ECD Electron capture detector

LHV Lower heating value

MAE Mean absolute error

MLP Multilayer perceptron

ML Machine learning

MSE Mean squared error

NDIR Non-dispersive infrared

O&M Operation and maintenance

ReLU Rectifier linear unit

RMSE Root mean squared error

SAE Simple averaging ensemble

SHAP Shapley additive explanations

TCD Thermal conductivity detector

WAE Weighted averaging ensemble

Acknowledgements

The authors deeply appreciate the technical support and assistance provided by IFAPA Centro "Venta del Llano".

References

[1] S. Sharma, S. Basu, N. P. Shetti, M. Kamali, P. Walvekar, T. M. Aminabhavi, Waste-to-energy nexus: A sustainable development, Environ. Pollut. 267 (2020) 115501. doi:10.1016/j.envpol.2020.115501.

[2] N. Indrawan, A. Kumar, M. Moliere, K. A. Sallam, R. L. Huhnke, Distributed power generation via gasification of biomass and municipal solid waste: A review, J. Energy Inst. 93 (6) (2020) 2293–2313. doi:10.1016/j.joei.2020.07.001.

[3] A. Kushwah, T. Reina, M. Short, Modelling approaches for biomass gasifiers: A comprehensive overview, Sci. Total Environ. 834 (2022) 155243. doi:10.1016/j.scitotenv.2022.155243.

[4] R. G. dos Santos, A. C. Alencar, Biomass-derived syngas production via gasification process and its catalytic conversion into fuels by Fischer Tropsch synthesis: A review, Int. J. Hydrog. Energy 45 (36) (2020) 18114–18132. doi:10.1016/j.ijhydene.2019.07.133.

[5] J. Makwana, A. Dhass, P. Ramana, D. Sapariya, D. Patel, An analysis of waste/biomass gasification producing hydrogen-rich syngas: A review, Int. J. Thermofluids 20 (2023) 100492. doi:10.1016/j.ijft.2023.100492.

[6] M. Fatiguso, A. R. Valenti, S. Ravelli, Comparative energy performance analysis of micro gas turbine and internal combustion engine in a cogeneration plant based on biomass gasification, J. Clean. Prod. (2023) 139782doi:10.1016/j.jclepro.2023.139782.

[7] F. Patuzzi, D. Prando, S. Vakalis, A. M. Rizzo, D. Chiaramonti, W. Tirler, T. Mimmo, A. Gasparella, M. Baratieri, Small-scale biomass gasification chp systems: Comparative performance assessment and monitoring experiences in south tyrol (italy), Energy 112 (2016) 285–293. doi:10.1016/j.energy.2016.06.077.

[8] F. Patuzzi, D. Basso, S. Vakalis, D. Antolini, S. Piazzi, V. Benedetti, E. Cordioli, M. Baratieri, State-of-the-art of small-scale biomass gasification systems: An extensive and unique monitoring review, Energy 223 (2021) 120039. doi:10.1016/j.energy.2021.120039.

[9] P. Basu, Biomass Gasification, Pyrolysis and Torrefaction, 3rd Edition, Academic Press, 2018. doi:10.1016/C2016-0-04056-1.

[10] A. Y. Mutlu, Ö. Yücel, An artificial intelligence based approach to predicting syngas composition for downdraft biomass gasification, Energy 165 (2018) 895–901. doi:10.1016/j.energy.2018.09.131.

[11] Y. Fang, L. Ma, Z. Yao, W. Li, S. You, Process optimization of biomass gasification with a Monte Carlo approach and random forest algorithm, Energy Convers. Manag. 264 (2022) 115734. doi:10.1016/j.enconman.2022.115734.

[12] D. S. Pandey, H. Raza, S. Bhattacharyya, Development of explainable AI-based predictive models for bubbling fluidised bed gasification process, Fuel 351 (2023) 128971. doi:10.1016/j.fuel.2023.128971.

[13] Y. Ögren, A. Sepman, E. Fooladgar, F. Weiland, H. Wiinikka, Development and evaluation of a vision driven sensor for estimating fuel feeding rates in combustion and gasification processes, Energy and AI 15 (2024) 100316. doi:10.1016/j.egyai.2023.100316.

[14] S. Hashem Samadi, B. Ghobadian, M. Nosrati, M. Rezaei, Investigation of factors affecting performance of a downdraft fixed bed gasifier using optimized MLP neural networks approach, Fuel 333 (2023) 126249. doi:10.1016/j.fuel.2022.126249.

[15] R. Mikulandrić, D. Lončar, D. Böhning, R. Böhme, M. Beckmann, Artificial neural network modelling approach for a biomass gasification process in fixed bed gasifiers, Energy Convers. Manag. 87 (2014) 1210–1223. doi:10.1016/j.enconman.2014.03.036.

[16] D. Baruah, D. Baruah, M. Hazarika, Artificial neural network based modeling of biomass gasification in fixed bed downdraft gasifiers, Biomass Bioenerg. 98 (2017) 264–271. doi:10.1016/j.biombioe.2017.01.029.

[17] O. Yucel, E. S. Aydin, H. Sadikoglu, Comparison of the different artificial neural networks in prediction of biomass gasification products, Int. J. Energy Res. 43 (11) (2019) 5992–6003. doi:10.1002/er.4682.

[18] F. Elmaz, Ö. Yücel, A. Y. Mutlu, Predictive modeling of biomass gasification with machine learning-based regression methods, Energy 191 (2020) 116541. doi:10.1016/j.energy.2019.116541.

[19] R. Aguado, J.-L. Casteleiro-Roca, D. Vera, J. L. Calvo-Rolle, A hybrid intelligent model to predict the hydrogen concentration in the producer gas from a downdraft gasifier, Int. J. Hydrog. Energy 47 (48) (2022) 20755–20770. doi:10.1016/j.ijhydene.2022.04.174.

[20] E. E. Ozbas, D. Aksu, A. Ongen, M. A. Aydin, H. K. Ozcan, Hydrogen production via biomass gasification, and modeling by supervised machine learning algorithms, Int. J. Hydrog. Energy 44 (32) (2019) 17260–17268. doi:10.1016/j.ijhydene.2019.02.108.

[21] M. Puig-Arnavat, J. A. Hernández, J. C. Bruno, A. Coronas, Artificial neural network models for biomass gasification in fluidized bed gasifiers, Biomass Bioenerg. 49 (2013) 279–289. doi:10.1016/j.biombioe.2012.12.012.

[22] D. S. Pandey, S. Das, I. Pan, J. J. Leahy, W. Kwapinski, Artificial neural network based modelling approach for municipal solid waste gasification in a fluidized bed reactor, Waste Manage. 58 (2016) 202–213. doi:10.1016/j.wasman.2016.08.023.

[23] J. George, P. Arun, C. Muraleedharan, Assessment of producer gas composition in air gasification of biomass using artificial neural network model, Int. J. Hydrog. Energy 43 (20) (2018) 9558–9568. doi:10.1016/j.ijhydene.2018.04.007.

[24] C. Sun, L. Ai, T. Liu, The PSO-ANN modeling study of highly valuable material and energy production by gasification of solid waste: an artificial intelligence algorithm approach, Biomass Conversion and Biorefinery 14 (2024) 2173–2184. doi:10.1007/s13399-022-02342-2.

[25] S. Ascher, W. Sloan, I. Watson, S. You, A comprehensive artificial neural network model for gasification process prediction, Appl. Energy 320 (2022) 119289. doi:10.1016/j.apenergy.2022.119289.

[26] G. C. Umenweke, I. C. Afolabi, E. I. Epelle, J. A. Okolie, Machine learning methods for modeling conventional and hydrothermal gasification of waste biomass: A review, Bioresource Technology Reports 17 (2022) 100976. doi:10.1016/j.biteb.2022.100976.

[27] S. Ascher, I. Watson, S. You, Machine learning methods for modelling the gasification and pyrolysis of biomass and waste, Renew. Sust. Energ. Rev. 155 (2022) 111902. doi:10.1016/j.rser.2021.111902.

[28] M. Khan, S. Raza Naqvi, Z. Ullah, S. Ali Ammar Taqvi, M. Nouman Aslam Khan, W. Farooq, M. Taqi Mehran, D. Juchelková, L. Štěpanec, Applications of machine learning in thermochemical conversion of biomass-A review, Fuel 332 (2023) 126055. doi:10.1016/j.fuel.2022.126055.

[29] O. Bongomin, C. Nzila, J. I. Mwasiagi, O. Maube, Exploring insights in biomass and waste gasification via

ensemble machine learning models and interpretability techniques, Int. J. Energy Res. 2024 (1) (2024) 6087208. doi:10.1155/2024/6087208.

[30] A. Jentzen, A. Riekert, A proof of convergence for the gradient descent optimization method with random initializations in the training of neural networks with ReLU activation for piecewise linear target functions, ArXiv abs/2108.04620 (2021).

[31] W. Wang, Some fundamental issues in ensemble methods (2008) 2243–2250doi:10.1109/IJCNN.2008.4634108.

[32] C.-H. Chen, K. Tanaka, M. Kotera, K. Funatsu, Comparison and improvement of the predictability and interpretability with ensemble learning models in QSPR applications, J. Cheminformatics 12 (1) (2020) 19. doi:10.1186/s13321-020-0417-9.

[33] Z. F. Wenjuan Feng, Jin Gou, X. Chen, An ensemble machine learning approach for classification tasks using feature generation, Connection Science 35 (1) (2023) 2231168. doi:10.1080/09540091.2023.2231168.

[34] N. Kardani, A. Zhou, M. Nazem, X. Lin, Modelling of municipal solid waste gasification using an optimised ensemble soft computing model, Fuel 289 (2021) 119903. doi:10.1016/j.fuel.2020.119903.

[35] J. Y. Kim, U. H. Shin, K. Kim, Predicting biomass composition and operating conditions in fluidized bed biomass gasifiers: An automated machine learning approach combined with cooperative game theory, Energy 280 (2023) 128138. doi:10.1016/j.energy.2023.128138.

[36] A. K. Sharma, Experimental study on 75 kW_{th} downdraft (biomass) gasifier system, Renew. Energy 34 (7) (2009) 1726–1733. doi:10.1016/j.renene.2008.12.030.

[37] Xiang Luo and Tao Wu and Kaiqi Shi and Mingxuan Song and Yusen Rao, Biomass gasification: An overview of technological barriers and socio-environmental impact, in: Y. Yun (Ed.), Gasification for Low-grade Feedstock, IntechOpen, Rijeka, 2018, Ch. 1. doi:10.5772/intechopen.74191.

[38] R. Aguado, A. Escámez, F. Jurado, D. Vera, Experimental assessment of a pilot-scale gasification plant fueled with olive pomace pellets for combined power, heat and biochar production, Fuel 344 (2023) 128127. doi:10.1016/j.fuel.2023.128127.

[39] M. Dogru, Experimental results of olive pits gasification in a fixed bed downdraft gasifier system, Int. J. Green Energy 10 (4) (2013) 348–361. doi:10.1080/15435075.2012.655351.

[40] Hubei Cubic-Ruiyi Instrument Co. Ltd., Portable Infrared Syngas Analyzer Gasboard 3100P User Manual, https://www.gas-analyzers.com/ProcessGasAnalyzer/info49/, accessed: November 9, 2023.

[41] C.-H. Shen, J.-H. Yeah, Long Term Stable Δ-Σ NDIR Technique Based on Temperature Compensation, Appl. Sci. 9 (2) (2019). doi:10.3390/app9020309.

[42] J. Hodgkinson, R. Smith, W. O. Ho, J. R. Saffell, R. P. Tatam, Non-dispersive infra-red (NDIR) measurement of carbon dioxide at 4.2μm in a compact and optically efficient sensor, Sensors and Actuators B: Chemical 186 (2013) 580–588. doi:10.1016/j.snb.2013.06.006.

[43] G. Ducom, J.-P. Tagutchou, M. Gautier, C. Gaignaire, J. Méhu, R. Gourdon, Olive mill solid waste gasification in a pilot-scale downdraft gasifier with three-stage air supply: performance, mass-energy balance and fate of inorganic elements, Fuel 340 (2023) 127469. doi:10.1016/j.fuel.2023.127469.

[44] D. Opitz, R. Maclin, Popular ensemble methods: An empirical study, Journal of Artificial Intelligence Research 11 (1999) 169–198. doi:10.1613/jair.614.
URL 10.1613/jair.614

[45] W. Wang, P. Jones, D. Partridge, Diversity between neural networks and decision trees for building multiple classifier systems (2000) 240–249doi:10.1007/3-540-45014-9_23.

[46] O. A. Montesinos López, A. Montesinos López, J. Crossa, Fundamentals of Artificial Neural Networks and Deep Learning, Springer International Publishing, Cham, 2022, pp. 379–425. doi:10.1007/978-3-030-89010-0_10.

[47] X. Glorot, A. Bordes, Y. Bengio, Deep sparse rectifier neural networks, in: G. Gordon, D. Dunson, M. Dudík (Eds.), Proceedings of the Fourteenth International Conference on Artificial Intelligence and Statistics, Vol. 15 of Proceedings of Machine Learning Research, PMLR, Fort Lauderdale, FL, USA, 2011, pp. 315–323.

[48] V. Nair, G. E. Hinton, Rectified linear units improve restricted boltzmann machines, in: Proceedings of the 27th International Conference on International Conference on Machine Learning, ICML'10, Omnipress, Madison, WI, USA, 2010, p. 807–814.

[49] R. Fernandes de Mello, M. Antonelli Ponti, A Brief Review on Machine Learning, Springer International Publishing, Cham, 2018, pp. 1–74. doi:10.1007/978-3-319-94989-5_1.

[50] F. Murtagh, Multilayer perceptrons for classification and regression, Neurocomputing 2 (5) (1991) 183–197. doi:10.1016/0925-2312(91)90023-5.

[51] S. Wang, Y. Zhang, C. Zhang, M. Yang, Improved artificial neural network method for predicting photovoltaic output performance, Global Energy Interconnection 3 (6) (2020) 553–561. doi:10.1016/j.gloei.2021.01.005.

[52] D. P. Kingma, J. Ba, Adam: A method for stochastic optimization, arXiv preprint arXiv:1412.6980 (2014). doi:10.48550/arXiv.1412.6980.

[53] D. Kingma, J. Ba, Adam: A method for stochastic optimization, International Conference on Learning Representations (12 2014).

[54] S. J. Reddi, S. Kale, S. Kumar, On the convergence of adam and beyond, ArXiv abs/1904.09237 (2018).
URL https://api.semanticscholar.org/CorpusID:3455897

[55] D. P. Kingma, M. Welling, Auto-encoding variational bayes (2022). arXiv:1312.6114.
URL https://arxiv.org/abs/1312.6114

[56] S. Ascher, X. Wang, I. Watson, W. Sloan, S. You, Interpretable machine learning to model biomass and waste gasification, Bioresour. Technol. 364 (2022) 128062. doi:10.1016/j.biortech.2022.128062.

[57] K. Kundu, A. Kumar, H. Kodamana, K. K. Pant, Obtaining high H_2-rich syngas yield and carbon conversion efficiency from biomass gasification: From characterization to process optimization using machine learning with experimental validation, Fuel 378 (2024) 132931. doi:10.1016/j.fuel.2024.132931.

[58] M. V. Shcherbakov, A. Brebels, N. L. Shcherbakova, A. P. Tyukov, T. A. Janovsky, V. A. Kamaev, A survey of forecast error measures, World Appl. Sci. J. 24 (2013) 171–176. doi:10.5829/idosi.wasj.2013.24.itmies.80032.

[59] M. Meena, H. Kumar, N. D. Chaturvedi, A. A. Kovalev, V. Bolshev, D. A. Kovalev, P. K. Sarangi, A. Chawade, M. S. Rajput, V. Vivekanand, V. Panchenko, Biomass gasification and applied intelligent retrieval in modeling, Energies 16 (18) (2023). doi:10.3390/en16186524.

[60] J. Li, L. Pan, M. Suvarna, X. Wang, Machine learning aided supercritical water gasification for h_2-rich syngas production with process optimization and catalyst screening, Chemical Engineering Journal 426 (2021) 131285. doi:10.1016/j.cej.2021.131285.

[61] G. D. Garson, Interpreting neural-network connection weights, AI expert 6 (4) (1991) 46–51.

[62] S. Safarian, S. M. Ebrahimi Saryazdi, R. Unnthorsson, C. Richter, Artificial neural network integrated with thermodynamic equilibrium modeling of downdraft biomass gasification-power production plant, Energy 213 (2020) 118800. doi:10.1016/j.energy.2020.118800.

[63] J. D. Olden, M. K. Joy, R. G. Death, An accurate comparison of methods for quantifying variable importance in artificial neural networks using simulated data, Ecological Modelling 178 (3) (2004) 389–397. doi:10.1016/j.ecolmodel.2004.03.013.

[64] M. V. Gil, K. M. Jablonka, S. Garcia, C. Pevida, B. Smit, Biomass to energy: a machine learning model for optimum gasification pathways, Digital Discovery 2 (2023) 929–940. doi:10.1039/D3DD00079F.